nanomaterials

MDPI

Article

Generation of Pure Green Up-Conversion Luminescence in Er^{3+} Doped and Yb^{3+}-Er^{3+} Co-Doped YVO_4 Nanomaterials under 785 and 975 nm Excitation

Natalia Stopikowska [1], Marcin Runowski [1,2,*], Przemysław Woźny [1], Stefan Lis [1] and Peng Du [3,*]

[1] Department of Rare Earths, Faculty of Chemistry, Adam Mickiewicz University, Uniwersytetu Poznańskiego 8, 61-614 Poznań, Poland; natalia.stopikowska@amu.edu.pl (N.S.); przemyslaw.wozny@amu.edu.pl (P.W.); blis@amu.edu.pl (S.L.)
[2] Departamento de Física, Universidad de La Laguna, Apartado de Correos 456, E-38200 San Cristóbal de La Laguna, Spain
[3] Department of Microelectronic Science and Engineering, School of Physical Science and Technology, Ningbo University, Ningbo 315211, China
* Correspondence: runowski@amu.edu.pl (M.R.); dupeng@nbu.edu.cn (P.D.)

Abstract: Materials that generate pure, single-color emission are desirable in the development and manufacturing of modern optoelectronic devices. This work shows the possibility of generating pure, green up-conversion luminescence upon the excitation of Er^{3+}-doped nanomaterials with a 785 nm NIR laser. The up-converting inorganic nanoluminophores YVO_4: Er^{3+} and YVO_4: Yb^{3+} and Er^{3+} were obtained using a hydrothermal method and subsequent calcination. The synthesized vanadate nanomaterials had a tetragonal structure and crystallized in the form of nearly spherical nanoparticles. Up-conversion emission spectra of the nanomaterials were measured using laser light sources with λ_{ex} = 785 and 975 nm. Importantly, under the influence of the mentioned laser irradiation, the as-prepared samples exhibited bright green up-conversion luminescence that was visible to the naked eye. Depending on the dopant ions used and the selected excitation wavelengths, two (green) or three (green and red) bands originating from erbium ions appeared in the emission spectra. In this way, by changing the UC mechanisms, pure green luminescence of the material can be obtained. The proposed strategy, in combination with various single-doped UC nanomaterials activated with Er^{3+}, might be beneficial for modern optoelectronics, such as light-emitting diodes with a rich color gamut for back-light display applications.

Keywords: lanthanide ions; up-conversion; nanomaterials; rare earth ions; pure green luminescence

Citation: Stopikowska, N.; Runowski, M.; Woźny, P.; Lis, S.; Du, P. Generation of Pure Green Up-Conversion Luminescence in Er^{3+} Doped and Yb^{3+}-Er^{3+} Co-Doped YVO_4 Nanomaterials under 785 and 975 nm Excitation. *Nanomaterials* **2022**, *12*, 799. https://doi.org/10.3390/nano12050799

Academic Editor: Lothar Wondraczek

Received: 2 February 2022
Accepted: 23 February 2022
Published: 26 February 2022

1. Introduction

Up-conversion (UC), anti-Stokes luminescence is a phenomenon where two or more low-energy photons are converted into one photon of higher energy. In this way, the accumulated energy in the system, usually absorbed by the sensitizer ions, is transferred to the activator ions [1–5]. In order to generate efficient UC luminescence, the inorganic matrices co-doped with rare earth ions (typically Ho^{3+}, Er^{3+} and Tm^{3+}) are commonly used, such as vanadates, phosphates, borates, fluorides, oxides etc. [1–3,6–16]. Currently, up-converting (nano)materials are commonly studied in terms of the components of solar cells [17], bioimaging [18,19], nanothemrometry [3,20–26], forensics [27], composite membranes etc. [28].

Rare-earth vanadates are a group of compounds that are used in many fields of science due to their favorable physicochemical properties, such as chemical stability, relatively low phonon energy (≈900 cm^{-1}) [29], lower cytotoxicity than quantum dots [30], simple and eco-friendly synthesis method [31–34] and so forth.

Importantly, the vanadate-based materials and nanomaterials have much better thermal stability (even above ≈1300 K), in contrast to their fluoride analogues (commonly

studied luminescent micron-sized and nano-sized particles), which begin to oxidize and decompose usually above ≈700 K [10,15,25–27,29].

Moreover, due to the doping of lanthanide ions (Ln^{3+}) in their internal structure, such materials are optically active, and may exhibit luminescence phenomena upon appropriate photoexcitation, showing characteristic, sharp and narrow emission bands, corresponding to the Ln^{3+} 4f-4f transitions [20,35]. The vanadate matrices are often used in the conventional luminescence research and also in UC emission studies. In the first case of generating UV-excited luminescence, the emitter ions are, e.g., Eu^{3+}, Pr^{3+}, Sm^{3+}, Dy^{3+}, Ho^{3+} and Nd^{3+} [36–44].

In the case of generation of the UC emission, the most frequently used dopant ions are the following systems: Yb^{3+}-Er^{3+}, Yb^{3+}-Tm^{3+} and Yb^{3+}-Ho^{3+}, [45–48]; however, triple or even four-fold doped systems are also known, such as Yb^{3+}-Ho^{3+}-Nd^{3+} and Yb^{3+}-Tm^{3+}-Ho^{3+}-Er^{3+} [49,50]. One of the most commonly studied materials is YVO_4 doped with Yb^{3+}-Er^{3+}. In the case of this system, scientists typically use a conventional NIR laser emitting wavelength of 975–980 nm to generate UC emission [27,31,51–56].

Woźny et al. reported the UC emission spectra for the YVO_4: Yb^{3+}-Er^{3+} obtained using the co-precipitation method, without the calcination process. In this case, the average size of the material was estimated at 21 nm, and an intense red emission band of Er^{3+} ($^4F_{9/2} \rightarrow {}^4I_{15/2}$ transition) located around 650 nm was observed in the emission spectrum (λ_{ex} = 975 nm) [57]. Szczeszak et al. obtained an analogous material using the Pechini method [58]. The material showed high agglomeration, and the average grain size was estimated at 20–50 nm. In that case, the same red emission band originating from Er^{3+} was also observed (λ_{ex} = 980 nm).

Meng et al. obtained YVO_4: Yb^{3+}-Er^{3+} material using the co-precipitation method [51]. They focused on synthesizing the vanadate materials with different grain sizes, i.e., particles with average sizes of 20 and 60 nm, as well as 1 µm. The research showed the effect of the material size on the intensity of the band coming from the mentioned Er^{3+} transition, i.e., $^4F_{9/2} \rightarrow {}^4I_{15/2}$. In this case, the intensity of the red band decreased with the increase of the particle size.

However, there are also reports about YVO_4: Yb^{3+}-Er^{3+} materials generating conventional (Stokes) emission, such as the contribution of T. Tsuboi, who investigated the absorption and emission characteristics of this material in the spectral ranges of 200–2000 and 400–1750 nm, respectively, using 671, 355 and 266 nm excitation wavelengths. This author observed not only the emission bands corresponding to Er^{3+} but also the emission band related to Yb^{3+} emission [57].

The discussed materials, based on vanadate matrices are also thermally very stable, [59–61], and therefore they are used as thermochromic phosphors, scintillators or optically active components of lasers [62] as well as contact-less temperature sensors [63,64], optical high pressure and vacuum sensors [29] and for fingerprint detection [27].

From the point of view of the use of nanomaterials in electronics and optoelectronics, their synthesis has many advantages, such as the possibility of preparation in large quantities with the desired composition, size, shape and structure reproducibility etc. During the preparation of vanadate, a water-based system is used, which provides a number of advantages, such as simplicity, safety, convenience, ease of transfer to large-scale production and no harmful organic solvents, which is very important from the point of view of green chemistry [31,62,65,66].

Here, we present the possibility of generating bright, green UC luminescence, from nanomaterials based on yttrium vanadate matrices doped with Er^{3+} or Yb^{3+}-Er^{3+} ions. The optically active compounds were obtained using a hydrothermal method and post-treatment calcination. The nanomaterials synthesized showed pure green up-conversion luminescence, which was clearly visible to the naked eye, under continuous laser excitations, alike at 785 nm (not widely used thus far) and 975 nm.

Importantly, in the case of 785 nm excitation, the emission spectrum of the single-doped nanomaterial (YVO_4: Er^{3+}) does not have any contribution of the red emission band

of Er^{3+} ($^4F_{9/2} \rightarrow {}^4I_{15/2}$ transition). Our studies show that the excitation wavelength and the presence of sensitizer ions play important roles in achieving pure green UC emission in vanadate nanomaterials.

These results and the developed strategy may be particularly important from the point of view of electronics and materials engineering, not only in utilizing vanadates but also other Er^{3+}-doped UC nanomaterials (e.g., molybdates and tungstates) excited at higher-energy NIR lasers. This is because the possibility of generating pure-color emission can be used for the manufacturing of modern optoelectronics, new light sources, optically active components of various devices etc.

2. Materials and Methods

2.1. Materials

RE_2O_3 (RE = Y^{3+}, Yb^{3+} and Er^{3+}) purchased from Stanford Materials (Stanford, CA, USA; 99.99%), were dissolved separately in 35–38% HCl from POCh. S.A. (Gliwice, Poland) to synthesize the corresponding $RECl_3$. Ammonium metavanadate (ACS reagent; ≥99.0%) and PEG 6000 were purchased from Sigma Aldrich (Darmstadt, Germany). Sodium hydroxide was purchased from POCh. S.A. (Gliwice, Poland, pure p.a.; 98.8%). Deionized water was used in each experiment.

We detail the synthesis of (A) YVO_4: 2% Er^{3+} and (B) YVO_4: 20% Yb^{3+} and 2% Er^{3+}. To synthesize 0.25 g of a given nanomaterial, the aqueous solutions of YCl_3 and $ErCl_3$ were mixed together in a molar ratio 0.98:0.02, i.e., 2.362 mL of 0.5 M YCl_3 and 0.048 mL of 0.5 M $ErCl_3$ for the product (A); and the aqueous solutions of YCl_3, $YbCl_3$ and $ErCl_3$ were mixed in a molar ratio 0.78:0.2:0.02, i.e., 1.739 mL of 0.5 M YCl_3, 0.446 mL of 0.5 M $YbCl_3$ and 0.045 mL of 0.5 M $ErCl_3$ for the product (B). Subsequently, 10 mL of water was added to the solutions of Ln^{3+} ions. Next, 0.25 g of PEG 6000 (anti-agglomeration agent) was added and dissolved in each of the as-prepared solutions.

The solutions containing vanadate ions were prepared by dissolving 0.141 g of NH_4VO_3 in 20 mL of water for the product (A); and 0.130 g of NH_4VO_3 for the product (B). An aqueous sodium hydroxide solution (15 mL) was added to each solution of ammonium metavanadate, at a molar ratio of 1:1. The solutions containing vanadate ions were heated up to 343 K to obtain transparent aqueous solutions and then added dropwise to the continuously stirred solutions of Ln^{3+}.

Then, water (up to 40 mL) was added to the as-prepared solutions, and, in the next step, the pH of each solution was adjusted to ≈ 10, using a 1.5 M solution of NaOH. The obtained mixtures were then transferred into Teflon-lined vessels and hydrothermally treated in an autoclave (for 18 h at 453 K).

Afterwards, the obtained white precipitates were dispersed several times in ethanol and water and centrifuged to purify the final products. The obtained products, i.e., YVO_4: Er^{3+} and YVO_4: Yb^{3+} and Er^{3+} were dried in an oven at 358 K for 15 h. Finally, the samples were ground in an agate mortar. Later, in order to enhance the crystallinity and the luminescence signal intensity of the products, they were calcined in a furnace for 4 h at 1173 K. After calcination, the products were ground again in an agate mortar.

2.2. Characterization

Powder X-ray diffraction patterns (XRD) were measured using a Bruker AXS D8 Advance diffractometer (Billerica, MA, USA) in Bragg–Brentano geometry (Cu Kα radiation λ = 0.15406 nm). Transmission electron microscopy (TEM) (Hitachi HT7700, Ltd. Tokyo, Japan) images were taken with a Hitachi HT7700 transmission electron microscope (100 kV accelerating voltage). An Andor Shamrock 500i spectrometer (Andor Technology Ltd., Belfast, UK), coupled with a silicon iDus CCD camera, working as a detector, was used for the emission spectra measurements. The samples were excited by the use of the fiber-coupled, solid-state diode pumped (SSDP) 975 and 785 nm lasers, i.e., FC-975-2W (CNI; Changchun, China) and LW-785-120-C12-DM (Lambdawave, Wrocław, Poland), respectively.

In both cases, the beam spot sizes were ≈200 µm (Gauss profile), and the laser power was adjusted to ≈100 mW, for both excitation wavelengths, which corresponds to the power densities of ≈50 W cm^{-2}. The luminescence decay curves were recorded using a 200 MHz Tektronix MDO3022 oscilloscope, coupled to the R928 PMT (Hamamatsu, Shimokanzo, Japan) and a QuantaMaster™ 40 spectrophotometer (Photon Technology International, Birmingham Rd, Birmingham UK). A tunable Opolette 355LD UVDM, nano-second pulsed laser, with a repetition rate of 20 Hz (Opotek Inc., Faraday Ave Suite E, Carlsbad, CA, USA), was used as the excitation source.

3. Results

3.1. Structure and Morphology

The recorded XRD patterns of the obtained nanomaterials: YVO_4: 2% Er^{3+} and YVO_4: 20% Yb^{3+} and 2% Er^{3+} (Figure 1a) agree with the reference pattern from the ICDD database (International Centre for Diffraction Data, card no. 01-082-1968) of the tetragonal YVO_4, crystallizing in the *I41/amd* space group. Due to the nanocrystallinity of the particles obtained, a significant broadening of reflexes was observed.

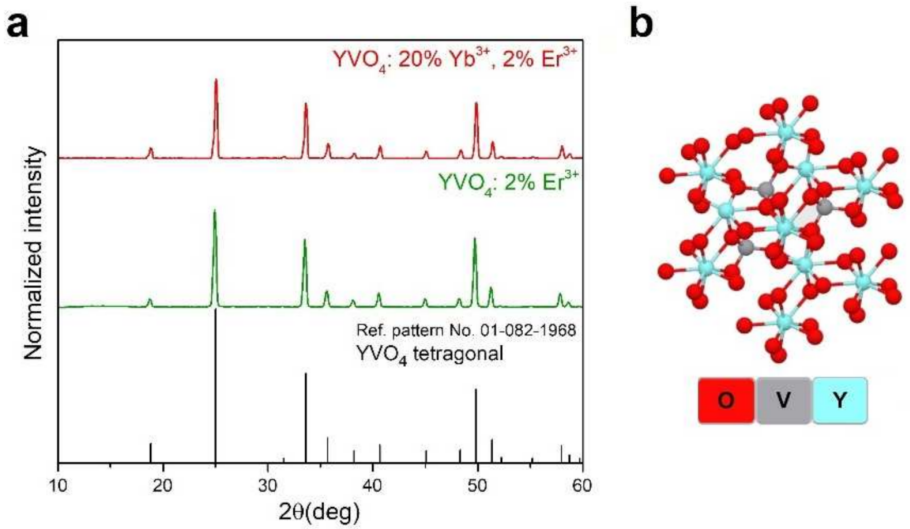

Figure 1. (**a**) Powder XRD patterns of the obtained YVO_4: 2% Er^{3+} and YVO_4: 20% Yb^{3+} and 2% Er^{3+} compounds and (**b**) a graphical representation of the arrangement of atoms in the crystal lattice of YVO_4.

Figure 1b shows a graphical representation of the arrangement of atoms in the synthesized crystal structures. In the cases of the Er^{3+} doped and Yb^{3+}-Er^{3+} co-doped YVO_4 materials, the Y^{3+} ions in the crystal lattice were partly substituted either by Er^{3+} ions or by Yb^{3+} and Er^{3+} ions, respectively. TEM images (Figure 2a,b) show that the obtained compounds were composed of irregular, agglomerated nanoparticles (NPs), and their average sizes were around 94 ± 32 nm for YVO_4: Er^{3+} (Figure 2c) and 66 ± 17 nm for YVO_4: Yb^{3+} and Er^{3+} (Figure 2d).

3.2. Luminescence Properties

The doping concentrations (20 mol.% of Yb^{3+} and 2 mol.% of Er^{3+}) were chosen based on our previous studies as well as the literature data [27,55,56]. This dopant ratio provides optimal, intense UC emissions, due to the efficient energy transfer process between Yb^{3+} and Er^{3+}. UC emission spectra were recorded in the range of 500–680 nm (Figure 3a; λ_{ex} = 785 or 975 nm; pump power density ≈ 50 W/cm^2). The synthesized nanomaterials exhibit a very bright green UC luminescence that is clearly visible to the naked eye.

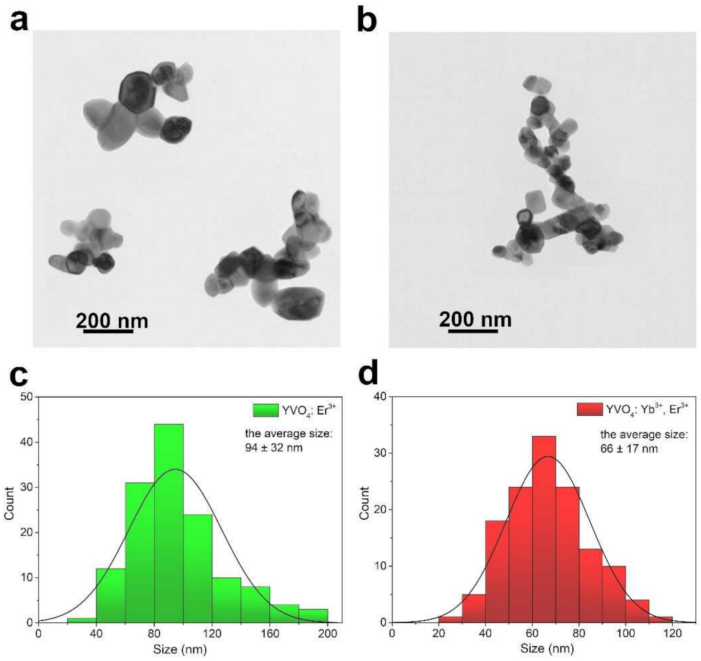

Figure 2. (**a**,**b**) TEM images and (**c**,**d**) corresponding size distribution histograms of the obtained nanomaterials, i.e., (**a**,**c**) YVO_4: Er^{3+} and (**b**,**d**) YVO_4: Yb^{3+} and Er^{3+}.

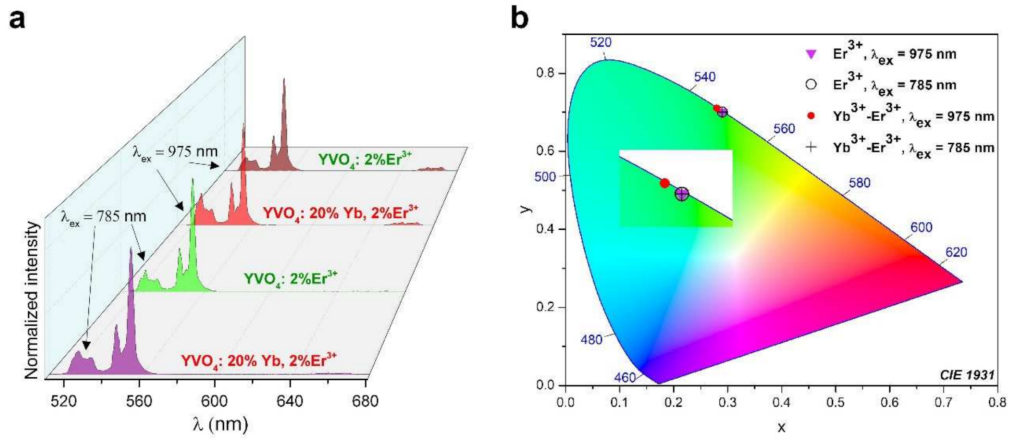

Figure 3. (**a**) Normalized UC emission spectra of the synthesized YVO_4: Er^{3+} and YVO_4: Yb^{3+} and Er^{3+} nanomaterials, measured at two different laser excitations (λ_{ex} = 785 or 975 nm; ≈50 W/cm^2) and (**b**) the corresponding chromaticity diagram (CIE 1931).

When using λ_{ex} = 785 nm, the emission spectrum of YVO_4: Er^{3+} consists of only two narrow, sharp bands from Er^{3+}: $^2H_{11/2} \rightarrow {}^4I_{15/2}$ (530 nm) and $^4S_{3/2} \rightarrow {}^4I_{15/2}$ (550 nm), associated with its *4f*−*4f* radiative transitions (both located in the green region of the spectrum). However, in the case of using λ_{ex} = 975 nm, the YVO_4: Er^{3+} and YVO_4: Yb^{3+} and Er^{3+} compounds exhibit an additional low intense band located around 670 nm, corresponding to the $^4F_{9/2} \rightarrow {}^4I_{15/2}$ transition of Er^{3+}. During the excitation of the co-doped nanomaterial YVO_4: Yb^{3+} and Er^{3+} with a 785 nm laser, a low-intensity band located around 670 nm was also visible. All bands are split into several Stark components due to the effects of the crystal-field.

In both synthesized nanomaterials YVO_4: Er^{3+} and YVO_4: Yb^{3+}-Er^{3+}, a pure green color of luminescence was achieved using λ_{ex} = 785 nm, as well as for the single-doped YVO_4:Er^{3+} (without ytterbium co-doping) excited at 975 nm, as presented in the chromaticity diagram in Figure 3b. However, for the nanomaterial YVO_4: Yb^{3+}-Er^{3+} excited at 975 nm, the resulting color coordinates are slightly shifted (see Figure 3b).

Based on the measured UC emission spectra, we determined the values of color coordinates, summarized in Table 1, where they are all on the edge of green region, and this indicates a higher color purity of the resulting emissions originating from the obtained nanomaterials. To confirm this deduction, we estimated the color purity utilizing the following equation [67,68]:

$$\text{Color purity} = \frac{\sqrt{(x - x_i)^2 + (y - y_i)^2}}{\sqrt{(x_d - x_i)^2 + (y_d - y_i)^2}} \times 100\% \quad (1)$$

where (x,y) denote the color coordinates of the developed nanoluminophores; (x_i,y_i) are the color coordinates of the white illuminate point, which have fixed values of (0.3101,0.3162) [69], and (x_d,y_d) are the color coordinates of the dominated emissions, whose values can be determined through extending the straight line between the points of (x,y) and (x_i,y_i) to the other side (edge of the CIE diagram) [70]. The determined values of (x_d,y_d) and color purities for the studied nanomaterials are summarized in Table 1.

Table 1. The values of color coordinates, color purity and CCT for the synthesized YVO_4: Er^{3+} and YVO_4: Yb^{3+} and Er^{3+} nanomaterials.

Dopants	λ_{ex} (nm)	Color Coordinates				Color Purity (%)	CCT (K)
		x	y	x_d	y_d		
Er^{3+}	785	0.2845	0.7022	0.2841	0.7066	98.9	6179
Er^{3+}	975	0.2937	0.6943	0.2934	0.6997	98.6	6055
Yb^{3+}, Er^{3+}	785	0.2965	0.6901	0.2966	0.6959	98.5	6018
Yb^{3+}, Er^{3+}	975	0.2731	0.7101	0.2722	0.7186	97.9	6334

As expected, the single-doped sample (YVO_4:Er^{3+}) excited at 785 nm reveals superior color purity of its green emission, namely, 98.9%. The color purity values change slightly with the manipulation of the chemical composition of the materials (dopant ions) and the excitation wavelengths. In addition to the color coordinates and color purity, the correlated color temperature (CCT) also plays an important role in determining the color properties of the generated emissions, and its value can be calculated using the following equations [70]:

$$\text{CCT} = -437n^3 + 3601n^2 - 6846n + 5514.31 \quad (2)$$

$$n = (x - x_e)/(y - y_e) \quad (3)$$

where (x_e,y_e) have fixed values of (0.3320,0.1858). Thereby, via using these aforementioned equations, the CCT values for the emissions of Er^{3+}-doped and Er^{3+}/Yb^{3+}-codoped YVO_4 nanomaterials excited with different wavelengths (785 or 975 nm) are calculated and presented in Table 1. As disclosed, by changing the dopant content and excitation wavelength, CCT values vary in the range of 6018 to 6334 K.

Additionally, it is worth noting that the intensity of the red emission band of Er^{3+} ($^4F_{9/2} \rightarrow {}^4I_{15/2}$) may also be influenced by the synthesis method of the luminescent material [51,52,55,71,72]. In general, based on the available literature data, it can be concluded that thermal treatment, i.e., high temperatures used during the solid-state method or post-synthesis calcination favor green emissions—namely, the relative intensity of the red emission band is significantly lower compared to the green emission bands [51,52,55,71,72].

Figure 4 shows how the selected excitation wavelengths and the elemental composition (single- or co-doped samples) affect the intensity of UC emission of the nanomaterials studied. The excitation of the samples at 785 nm, resulted in higher UC emission intensity for the single-doped YVO_4:Er^{3+} compound. This is most plausibly because, in the case of a co-doped material, after the excited state absorption of Er^{3+}, some of the excitation energy is transferred back to the Yb^{3+} ions, namely, via $Er^{3+} \rightarrow Yb^{3+}$ back energy transfer (BET),

which may further relax non-radiatively and radiatively (NIR emission of Yb^{3+}), resulting in a decrease in the intensity of Er^{3+} UC emission.

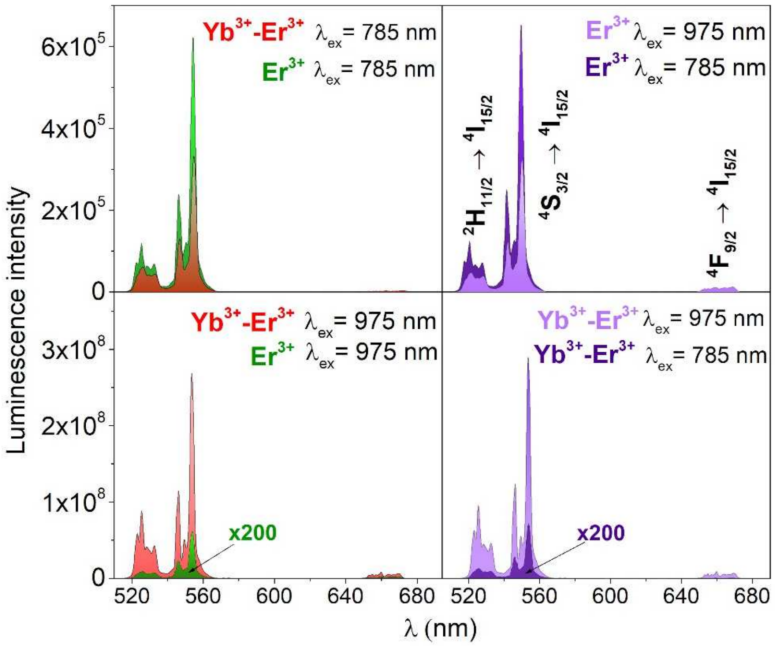

Figure 4. Non-normalized UC emission spectra of the obtained nanomaterials YVO_4: Er^{3+} and YVO_4: Yb^{3+}-Er^{3+}; λ_{ex} = 785 or 975 nm (≈50 W/cm^2).

While, as expected, the most intense UC luminescence is shown by the material co-doped with Yb^{3+}-Er^{3+} ions, excited at 975 nm—namely, two orders of magnitude higher compared to the second excitation wavelength and the single-doped sample (see Figure 4). This is due to the high absorption cross-section of Yb^{3+} in the NIR range, centered around 975 nm ($^2F_{7/2} \rightarrow {}^2F_{5/2}$ transitions of Yb^{3+}) and the effective energy transfer UC (ETU) from the sensitizing Yb^{3+} ions to the emitting Er^{3+} ions ($Yb^{3+} \rightarrow Er^{3+}$ ETU).

Importantly, using the 785 nm laser (allowing generation of the pure green luminescence), it is possible to excite the samples in the range of the first biological window (I-BW), i.e., 650–950 nm [3,7,13]. In this range, the disturbing factors, including scattering or/and absorption of the laser beam by the biological tissues, are less pronounced, allowing for better penetration of the tissue by the excitation beam. This feature is particularly important, e.g., in the field of development of optical contactless nano-thermometers, which are particularly useful in biological and medical research and applications [7,13,20].

According to the available literature data, the up-converting materials obtained thus far, based on the Er^{3+} doped or Yb^{3+}-Er^{3+} co-doped inorganic compounds do not show pure, green emission (without the influence of the red emission band) under the NIR laser excitation, i.e., in the I-BW spectral range. Table 2 summarizes the spectral characteristics of the luminescent nanomaterials based on the Er^{3+} emission in the vanadate matrices, among which, YVO_4 is the most commonly used host.

To date, pure green emission could be achieved only in the case of the conventional, UV-excited, down-shifting phosphors. Whereas, in the case of the up-converting materials, excited either in the I-BW or beyond, the red band was inherently present in the emission spectra.

The main radiative and non-radiative processes occurring in the studied nanomaterials are shown in Figure 5. In the case of the commonly studied systems, which are the Yb^{3+}-Er^{3+} co-doped UC phosphor excited at 975 nm, the already discussed and well-established ETU mechanism dominates (Figure 5d) [2,84–88]. On the other hand, for the single-doped materials (a,c), co-doped materials (b) excited at 785 nm, the mechanisms responsible for

UC emission of Er^{3+} are predominantly ground state absorption (GSA) and excited state absorption (ESA) processes.

Table 2. Comparison of spectral characteristics of different Er^{3+}-activated luminescent materials, based on the vanadate matrices.

Host	Dopant Ions	Detectable Red Emission Band	λ_{ex} (nm)	Excitation in the I-BW	Refs.
YVO_4	Er^{3+}	No	785	Yes	This work
	Er^{3+}	Yes	975	No	
	Yb^{3+}-Er^{3+}	Yes	785	Yes	
	Yb^{3+}-Er^{3+}	Yes	975	No	
YVO_4	Er^{3+}	Yes	305–340	No	[73]
	Yb^{3+}-Er^{3+}	Yes	290–330	No	
YVO_4	Er^{3+}	No	223	No	[74]
YVO_4	Er^{3+}	Yes	310	No	[75]
YVO_4	Er^{3+}	No	300	No	[76]
YVO_4	Er^{3+}	No	317	No	[77]
YVO_4	Yb^{3+}-Er^{3+}	Yes	980	No	[51]
YVO_4	Yb^{3+}-Er^{3+}	Yes	975	No	[57]
YVO_4	Yb^{3+}-Er^{3+}	Yes	980	No	[78]
YVO_4	Yb^{3+}-Er^{3+}	Yes	985	No	[31]
YVO_4	Yb^{3+}-Er^{3+}	Yes	970	No	[79]
YVO_4	Yb^{3+}-Er^{3+}	Yes	980	No	[54]
YVO_4	Yb^{3+}-Er^{3+}	Yes	980	No	[80]
YVO_4	Yb^{3+}-Er^{3+}	Yes	980	No	[28]
YVO_4	Yb^{3+}-Er^{3+}	Yes	980	No	[81]
YVO_4	Yb^{3+}-Er^{3+}	No	257	No	[82]
	Yb^{3+}-Er^{3+}	Yes	980	No	
$Ba_2GdV_3O_{11}$	Yb^{3+}-Er^{3+}	Yes	978	No	[62]
$K_3Y(VO_4)_2$	Yb^{3+}-Er^{3+}	Yes	980	No	[60]
$GdVO_4$	Yb^{3+}-Er^{3+}	Yes	980	No	[83]

In the latter case (b), the ETU mechanism may also contribute; however, it appears to be less efficient compared to the GSA and ESA mechanisms. Importantly, pure green luminescence, i.e., no red emission band in the spectrum, can only be fully achieved for a single-doped nanomaterial excited at 785 nm (directly into the $^4I_{9/2}$ level of Er^{3+}). This is because, only in that case (a), the $^4F_{9/2}$ level cannot be effectively populated (at least at room temperature), as evidenced by the measured spectra and energy level diagrams depicted.

The only way to theoretically populate this level would be a multi-phonon relaxation (from the $^4S_{3/2}$ level), which is often considered in the literature to be responsible for the red emission of Er^{3+} [2,85,86]. However, as the $^4S_{3/2}$ and $^4F_{9/2}$ levels are separated by $\approx$3000 cm^{-1}, at least four phonons are required to populate the lower-lying state (assuming the highest-energy phonon mode is $\approx$ 900 cm^{-1} in the vanadate crystal lattice), which evidently makes the mentioned multi-phonon relaxation process less efficient, compared to the competing green emission from the $^4S_{3/2}$ state in the system studied. Whereas, in other cases (b–d), a red emission band can be observed because the $^4F_{9/2}$ level can be populated via the ESA mechanism from the $^4I_{13/2}$ level (see the energy level diagrams in Figure 5).

In order to confirm the validity of the postulated UC emission mechanisms, we measured the UC emission decay curves for the YVO_4: Er^{3+} and YVO_4: Yb^{3+}-Er^{3+} nanomaterials, excited at λ_{ex} = 785 or 975 nm; monitored at λ_{em} = 530 (a), 550 (b) and 660 nm (c), which are presented in Figure 6. It is clear that, in the case of the samples co-doped with Yb^{3+}-Er^{3+} ions (violet and red curves), the ETU mechanism dominates in the UC processes, which is manifested by the appearance of the rise curve in the initial parts of the curve profiles (with maximum intensity around $\approx$3–4 μs).

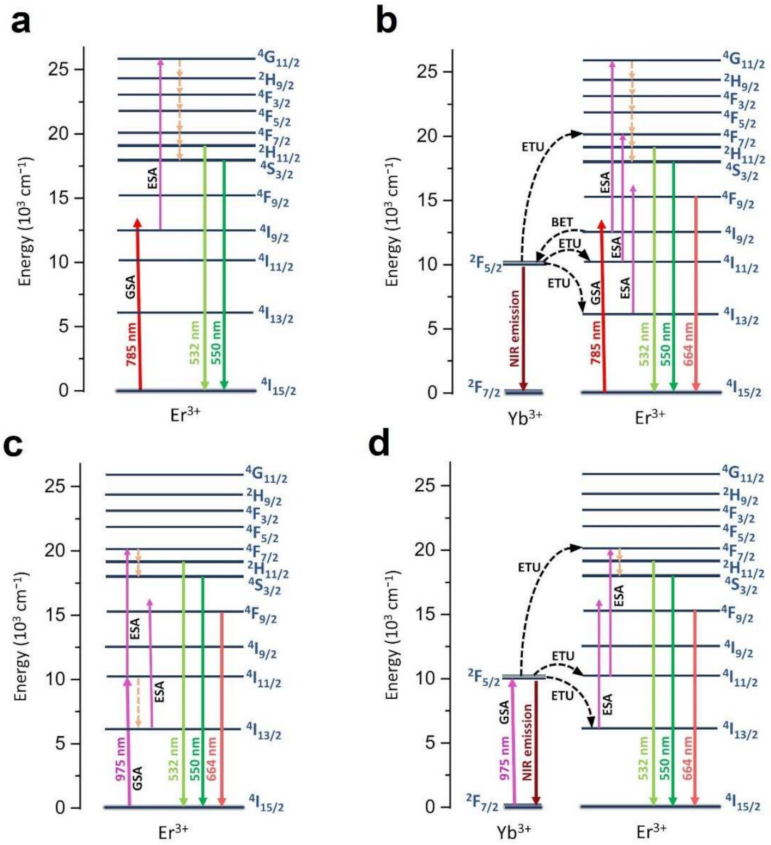

Figure 5. Energy level diagrams showing the main radiative (continuous lines) and non-radiative (dashed lines) processes occurring in the nanomaterials studied, i.e., (**a**) YVO_4: Er^{3+}, λ_{ex} = 785 nm; (**b**) YVO_4: Yb^{3+}-Er^{3+}, λ_{ex} = 785 nm; (**c**) YVO_4: Er^{3+}, λ_{ex} = 975 nm; (**d**) YVO_4: Yb^{3+}-Er^{3+}, λ_{ex} = 975 nm.

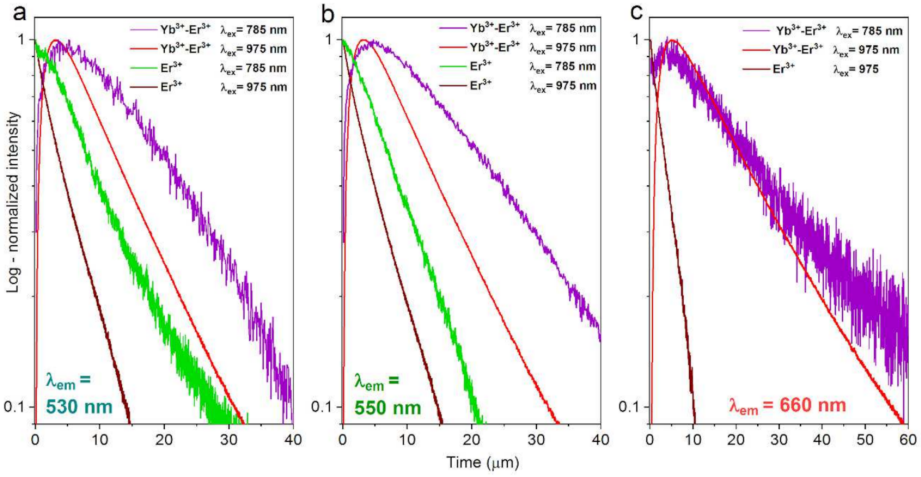

Figure 6. Normalized UC emission decay curves for the YVO_4: Er^{3+} and YVO_4: Yb^{3+}-Er^{3+} nanomaterials, excited at λ_{ex} = 785 or 975 nm; monitored at λ_{em} = 530 (**a**), 550 (**b**) and 660 nm (**c**).

Whereas, in the case of the single-doped samples, containing only Er^{3+} ions, we observe only simple decay profiles, without any rise component, alike at 975 and 785 nm excitations, confirming the dominant contribution of the GSA and ESA mechanisms. Note, the rise curves/components, which are typically observed in many up-converting materials, are related to the energy transfer from the sensitizer (light harvesting ion) to the emitting ions, which, in our case, are Yb^{3+} and Er^{3+} ions, respectively.

The deviations from the pure exponential character of the recorded luminescence decay curves are mainly due to the quenching effects, such as interionic cross-relaxation processes. That is why we simply used the following equation to estimate the average UC emission lifetimes for all observed transitions in the studied systems:

$$\tau = \frac{\int I(t) \cdot t dt}{\int I(t) dt} \quad (4)$$

where τ is the average decay time of UC luminescence and *I(t)* is the intensity at time *t*. The calculated lifetime values are given in Table 3. As expected, in the case of the Yb^{3+}-Er^{3+} co-doped systems the UC lifetimes are much longer (≈11–24 μs) compared to the ones doped only with Er^{3+} (≈3–8 μs).

Table 3. Determined average UC emission lifetimes for the YVO_4: Er^{3+} and YVO_4: Yb^{3+}-Er^{3+} nanomaterials (excited at λ_{ex} = 785 or 975 nm) for the transitions $^2H_{11/2} \rightarrow {}^4I_{15/2}$, $^4S_{3/2} \rightarrow {}^4I_{15/2}$ and $^4F_{9/2} \rightarrow {}^4I_{15/2}$.

Dopant Ions (λ Excitation)	UC Luminescence Lifetimes (τ) for the Transitions		
	$^2H_{11/2} \rightarrow {}^4I_{15/2}$ (530 nm)	$^4S_{3/2} \rightarrow {}^4I_{15/2}$ (550 nm)	$^4F_{9/2} \rightarrow {}^4I_{15/2}$ (660 nm)
Yb^{3+}-Er^{3+} (975 nm)	11.35 μs	11.66 μs	19.38 μs
Yb^{3+}-Er^{3+} (785 nm)	20.12 μs	20.76 μs	24.26 μs
Er^{3+} (975 nm)	3.37 μs	3.58 μs	3.05 μs
Er^{3+} (785 nm)	7.73 μs	7.01 μs	-

This is simply due to the presence of Yb^{3+} in the first case (the intrinsic lifetime of the Yb^{3+} $^2F_{5/2}$ excited state), and the related energy transfer to the emitting Er^{3+} ions, leading to the overall prolongation of the lifetimes. On the other hand, the UC lifetimes are almost twice as long for the systems excited with 785 nm laser (higher energy), compared to the 975 nm excitation. This is plausibly due to the excitation of the electrons to higher excited states ($^4G_{11/2}$) with a 785 nm laser (see Figure 5), subsequently leading to the longer relaxation time (via more intermediate excited states) to the emitting levels.

In order to determined and confirm the number of photons required for UC processes in the systems studied, the dependences of the integrated luminescence intensity (for each emission band) on the applied laser power were investigated and are presented as log–log plots in Figure 7. As expected, all emission bands of Er^{3+} were associated with two-photon transitions, both for λ_{ex} = 785 nm and λ_{ex} = 975 nm, alike for the single- and co-doped nanomaterials, as evidenced by the determined slope values, which are significantly higher than unity (one-photon process), being typically close to the ideal value of two (two-photon process).

The observed deviations from the ideal value (2) are common to UC materials, and they are typically associated with the processes of non-radiative quenching of the excited states of Er^{3+}, such as multi-phonon relaxation and cross-relaxation phenomena [9]. To determine the number of photons participating in the transitions associated with the observed UC emission bands, we used the well-known relation $I_{UC} \propto (I_{pump})^n$. In this relation, I_{UC} is the UC emission intensity, I_{pump} is the pump laser power density, and n is the number of photons involved in the UC mechanism. Performing a simple linear fitting, *n* can be calculated from the slopes of the plotted UC emission intensity as a function of the pump power in both the logarithmic representations [89–91].

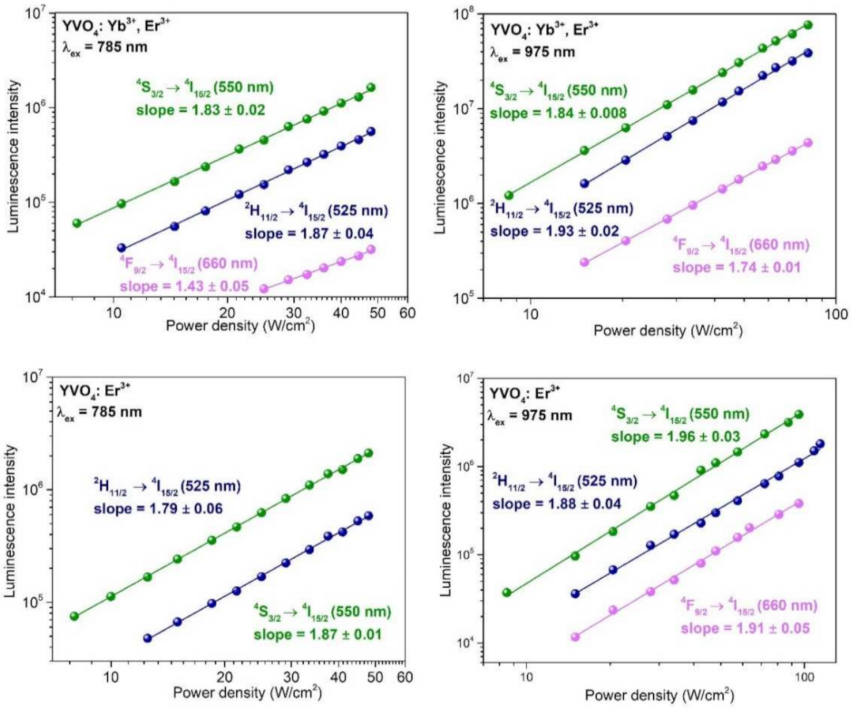

Figure 7. The log–log plots showing the dependences of the integrated UC luminescence intensity on the laser power for the samples YVO_4: Er^{3+} and YVO_4: Yb^{3+}-Er^{3+}. The determined slope values (by linear fitting) correspond to the number of photons participating in the particular transitions.

4. Conclusions

Here, we demonstrated the possibility of generating pure green UC emission by changing the UC mechanisms via manipulating the excitation wavelengths and the elemental composition of the dopants, thereby, resulting in altered energy migration pathways and ET processes. We achieved this goal by suppressing the population of the $^4F_{9/2}$ level of Er^{3+} in inorganic, vanadate-based up-converting nanoparticles.

The nanomaterials of interest were single- or co-doped YVO_4: Er^{3+} and YVO_4: Yb^{3+}-Er^{3+}, respectively, obtained by a combination of hydrothermal and calcination methods. The synthesized compounds showed intense, visible to the naked eye green UC luminescence that was observable at various excitation wavelengths, i.e., λ_{ex} = 785 nm or λ_{ex} = 975 nm. The influence of the excitation wavelength and elemental composition on the intensity of the UC emission was investigated.

This study showed that, in order to obtain pure green UC emission (without any contribution of the red emission band in the spectrum) from the Er^{3+}-doped inorganic matrices, the optically active phase should not contain Yb^{3+} ions and should be excited with higher-energy NIR light, such as a 785 nm laser, instead of the commonly used 975/980 nm lasers. The proposed strategy might be particularly important from the point of view of optoelectronics, lighting techniques, energy conversion etc.—in other words, whenever it is desired to generate light with a pure, single color.

Author Contributions: Conceptualization, N.S. and M.R.; methodology, N.S. and M.R.; validation, P.W.; formal analysis, N.S.; investigation, N.S., M.R. and P.D.; resources, N.S., P.W. and S.L.; data curation, P.W.; writing—original draft preparation, N.S.; writing—review and editing, M.R., S.L. and P.D.; visualization, P.W.; supervision, S.L. and M.R.; project administration, M.R.; funding acquisition, N.S. All authors have read and agreed to the published version of the manuscript.

Funding: This work was supported by the Polish National Science Centre (grant No. UMO-2018/31/N/ST4/00684).

Institutional Review Board Statement: Not applicable.

Informed Consent Statement: Not applicable.

Data Availability Statement: All of the relevant data are available from the correspondence authors upon reasonable request. Source data are provided with this paper.

Acknowledgments: Natalia Stopikowska is a recipient of the Adam Mickiewicz University Foundation scholarship for the academic year 2021/2022.

Conflicts of Interest: The authors declare no conflict of interest.

References

1. Runowski, M.; Shyichuk, A.; Tymiński, A.; Grzyb, T.; Lavín, V.; Lis, S. Multifunctional Optical Sensors for Nanomanometry and Nanothermometry: High-Pressure and High-Temperature Upconversion Luminescence of Lanthanide-Doped Phosphates—$LaPO_4/YPO_4$:Yb^{3+}-Tm^{3+}. *ACS Appl. Mater. Interfaces* **2018**, *10*, 17269–17279. [CrossRef] [PubMed]
2. Nadort, A.; Zhao, J.; Goldys, E.M. Lanthanide Upconversion Luminescence at the Nanoscale: Fundamentals and Optical Properties. *Nanoscale* **2016**, *8*, 13099–13130. [CrossRef] [PubMed]
3. Runowski, M.; Stopikowska, N.; Szeremeta, D.; Goderski, S.; Skwierczyńska, M.; Lis, S. Upconverting Lanthanide Fluoride Core@Shell Nanorods for Luminescent Thermometry in the First and Second Biological Windows: β-$NaYF_4$:Yb^{3+}—Er^{3+} @SiO_2 Temperature Sensor. *ACS Appl. Mater. Interfaces* **2019**, *11*, 13389–13396. [CrossRef]
4. Lim, C.S.; Aleksandrovsky, A.; Molokeev, M.; Oreshonkov, A.; Atuchin, V. Microwave Sol-Gel Synthesis and Upconversion Photoluminescence Properties of $CaGd_2(WO_4)_4$:Er^{3+}/Yb^{3+} Phosphors with Incommensurately Modulated Structure. *J. Solid State Chem.* **2015**, *228*, 160–166. [CrossRef]
5. Lim, C.S.; Aleksandrovsky, A.; Molokeev, M.; Oreshonkov, A.; Atuchin, V. Structural and Spectroscopic Effects of Li^+ Substitution for Na^+ in $Li_xNa_{1-}XCaGd_{0.5}Ho_{0\cdot05}Yb_{0\cdot45}(MoO_4)_3$ Scheelite-Type Upconversion Phosphors. *Molecules* **2021**, *26*, 7357. [CrossRef]
6. Marciniak, L.; Bednarkiewicz, A.; Stefanski, M.; Tomala, R.; Hreniak, D.; Strek, W. Near Infrared Absorbing near Infrared Emitting Highly-Sensitive Luminescent Nanothermometer Based on Nd^{3+} to Yb^{3+} Energy Transfer. *Phys. Chem. Chem. Phys.* **2015**, *17*, 24315–24321. [CrossRef] [PubMed]
7. Benayas, A. *Near Infrared-Emitting Nanoparticles for Biomedical Applications*; Springer: Cham, Switzerland, 2020. [CrossRef]
8. Hernández-Rodríguez, M.A.; Lozano-Gorrín, A.D.; Martín, I.R.; Rodríguez-Mendoza, U.R.; Lavín, V. Comparison of the Sensitivity as Optical Temperature Sensor of Nano-Perovskite Doped with Nd^{3+} Ions in the First and Second Biological Windows. *Sensors Actuators, B Chem.* **2018**, *255*, 970–976. [CrossRef]
9. Runowski, M.; Goderski, S.; Przybylska, D.; Grzyb, T.; Lis, S.; Martín, I.R. Sr_2LuF_7:Yb^{3+}-Ho^{3+}-Er^{3+} Upconverting Nanoparticles as Luminescent Thermometers in the First, Second, and Third Biological Windows. *ACS Appl. Nano Mater.* **2020**, *3*, 6406–6415. [CrossRef]
10. Gao, W.; Dong, J.; Liu, J.; Yan, X. Enhancement of Red Upconversion Emission of Cubic Phase $NaLuF_4$: Yb^{3+}/Ho^{3+}/Ce^{3+} Nanocrystals. *Mater. Res. Bull.* **2016**, *80*, 256–262. [CrossRef]
11. Zhou, Y.; He, X.H.; Yan, B. Self-Assembled $RE_2(MO_4)_3$:Ln^{3+} (RE = Y, La, Gd, Lu; M = W, Mo; Ln = Yb/Er, Yb/Tm) Hierarchical Microcrystals: Hydrothermal Synthesis and up-Conversion Luminescence. *Opt. Mater.* **2014**, *36*, 602–607. [CrossRef]
12. Oh, J.H.; Moon, B.K.; Choi, B.C.; Jeong, J.H.; Kim, J.H.; Lee, H.S. The Green Upconversion Emission Mechanism Investigation of $GdVO_4$:Yb^{3+}, Er^{3+} via Tuning of the Sensitizer Concentration. *Solid State Sci.* **2015**, *42*, 1–5. [CrossRef]
13. Kamimura, M.; Matsumoto, T.; Suyari, S.; Umezawa, M.; Soga, K. Ratiometric Near-Infrared Fluorescence Nanothermometry in the OTN-NIR (NIR II/III) Biological Window Based on Rare-Earth Doped β-$NaYF_4$ Nanoparticles. *J. Mater. Chem. B* **2017**, *5*, 1917–1925. [CrossRef] [PubMed]
14. Xia, T.; Cui, Y.; Yang, Y.; Qian, G. A Luminescent Ratiometric Thermometer Based on Thermally Coupled Levels of a Dy-MOF. *J. Mater. Chem. C* **2017**, *5*, 5044–5047. [CrossRef]
15. Singh, S.K.; Kumar, K.; Rai, S.B. Er^{3+}/Yb^{3+} Codoped Gd_2O_3 Nano-Phosphor for Optical Thermometry. *Sens. Actuators A Phys.* **2009**, *149*, 16–20. [CrossRef]
16. Dong, B.; Liu, D.P.; Wang, X.J.; Yang, T.; Miao, S.M.; Li, C.R. Optical Thermometry through Infrared Excited Green Upconversion Emissions in Er^{3+}—Yb^{3+} Codoped Al_2O_3. *Appl. Phys. Lett.* **2007**, *90*, 3–6. [CrossRef]
17. Chen, Z.; Jia, H.; Sharafudeen, K.; Dai, W.; Liu, Y.; Dong, G.; Qiu, J. Up-Conversion Luminescence from Single Vanadate through Blackbody Radiation Harvesting Broadband near-Infrared Photons for Photovoltaic Cells. *J. Alloys Compd.* **2016**, *663*, 204–210. [CrossRef]
18. Liu, Q.; Feng, W.; Li, F. Water-Soluble Lanthanide Upconversion Nanophosphors: Synthesis and Bioimaging Applications in Vivo. *Coord. Chem. Rev.* **2014**, *273–274*, 100–110. [CrossRef]
19. Tsang, M.K.; Chan, C.F.; Wong, K.L.; Hao, J. Comparative Studies of Upconversion Luminescence Characteristics and Cell Bioimaging Based on One-Step Synthesized Upconversion Nanoparticles Capped with Different Functional Groups. *J. Lumin.* **2015**, *157*, 172–178. [CrossRef]
20. Stopikowska, N.; Runowski, M.; Woźny, P.; Goderski, S.; Lis, S. Improving Temperature Resolution of Luminescent Nanothermometers Working in the Near-Infrared Range Using Non-Thermally Coupled Levels of Yb^{3+} & Tm^{3+}. *J. Lumin.* **2020**, *228*, 117643. [CrossRef]

21. Runowski, M. *Pressure and Temperature Optical Sensors: Luminescence of Lanthanide-Doped Nanomaterials for Contactless Nanomanometry and Nanothermometry*; Elsevier: Amsterdam, The Netherlands, 2019. [CrossRef]
22. Jaque, D.; Vetrone, F. Luminescence Nanothermometry. *Nanoscale* **2012**, *4*, 4301–4326. [CrossRef]
23. Dačanin, L.R.; Lukić-Petrović, S.R.; Petrović, D.M.; Nikolić, M.G.; Dramićanin, M.D. Temperature Quenching of Luminescence Emission in Eu^{3+}- and Sm^{3+}-Doped $YNbO_4$ Powders. *J. Lumin.* **2014**, *151*, 82–87. [CrossRef]
24. Brites, C.D.S.; Millán, A.; Carlos, L.D. Lanthanides in Luminescent Thermometry. *Handb. Phys. Chem. Rare Earths* **2016**, *49*, 339–427. [CrossRef]
25. Brites, C.D.S.; Fiaczyk, K.; Ramalho, J.F.C.B.; Sójka, M.; Carlos, L.D.; Zych, E. Widening the Temperature Range of Luminescent Thermometers through the Intra- and Interconfigurational Transitions of Pr^{3+}. *Adv. Opt. Mater.* **2018**, *6*, 1–5. [CrossRef]
26. Brites, C.D.S.; Lima, P.P.; Silva, N.J.O.; Millán, A.; Amaral, V.S.; Palacio, F.; Carlos, L.D. Thermometry at the Nanoscale. *Nanoscale* **2012**, *4*, 4799–4829. [CrossRef]
27. Ma, R.; Shimmon, R.; McDonagh, A.; Maynard, P.; Lennard, C.; Roux, C. Fingermark Detection on Non-Porous and Semi-Porous Surfaces Using YVO_4:Er,Yb Luminescent Upconverting Particles. *Forensic Sci. Int.* **2012**, *217*, 22–25. [CrossRef]
28. Nigoghossian, K.; Peres, M.F.S.; Primo, F.L.; Tedesco, A.C.; Pecoraro, E.; Messaddeq, Y.; Ribeiro, S.J.L. Infrared to Visible Up-Conversion in Biocellulose-Yttrium Vanadate Nanoparticle Composite Membranes: Demonstration of Chloroaluminum Phthalocyanine Light Emission Under Up-Converted Light Excitation. *Colloids Interface Sci. Commun.* **2014**, *2*, 6–10. [CrossRef]
29. Runowski, M.; Woźny, P.; Lis, S.; Lavín, V.; Martín, I.R. Optical Vacuum Sensor Based on Lanthanide Upconversion—Luminescence Thermometry as a Tool for Ultralow Pressure Sensing. *Adv. Mater. Technol.* **2020**, *5*, 1–8. [CrossRef]
30. Derfus, A.M.; Chan, W.C.W.; Bhatia, S.N. Probing the Cytotoxicity of Semiconductor Quantum Dots. *Nano Lett.* **2004**, *4*, 11–18. [CrossRef]
31. Woźny, P.; Szczeszak, A.; Lis, S. Effect of Various Surfactants on Changes in the Emission Color Chromaticity in Upconversion YVO_4: Yb^{3+}, Er^{3+} Nanoparticles. *Opt. Mater.* **2018**, *76*, 400–406. [CrossRef]
32. Zeng, L.; Pan, Y.; Zou, R.; Zhang, J.; Tian, Y.; Teng, Z.; Wang, S.; Ren, W.; Xiao, X.; Zhang, J.; et al. 808 Nm-Excited Upconversion Nanoprobes with Low Heating Effect for Targeted Magnetic Resonance Imaging and High-Efficacy Photodynamic Therapy in HER2-Overexpressed Breast Cancer. *Biomaterials* **2016**, *103*, 116–127. [CrossRef]
33. Toma, O.; Georgescu, S. Excited-State Absorption in Erbium-Doped Calcium Lithium Niobium Gallium Garnet. *J. Lumin.* **2014**, *154*, 553–558. [CrossRef]
34. Collins, J.; Geen, M.; Bettinelli, M.; Di Bartolo, B. Dependence of Cross-Relaxation on Temperature and Concentration from the $^1D_2$ Level of Pr^{3+} in YPO_4. *J. Lumin.* **2012**, *132*, 2626–2633. [CrossRef]
35. Runowski, M.; Stopikowska, N.; Lis, S. UV-Vis-NIR Absorption Spectra of Lanthanide Oxides and Fluorides. *Dalt. Trans.* **2020**, *49*, 2129–2137. [CrossRef] [PubMed]
36. Yanhong, L.; Guangyan, H. Synthesis and Luminescence Properties of Nanocrystalline YVO_4:Eu^{3+}. *J. Solid State Chem.* **2005**, *178*, 645–649. [CrossRef]
37. Mahlik, S.; Grinberg, M.; Cavalli, E.; Bettinelli, M.; Boutinaud, P. High Pressure Evolution of YVO_4:Pr^{3+} Luminescence. *J. Phys. Condens. Matter* **2009**, *21*, 105401. [CrossRef]
38. Riwotzki, K.; Haase, M. Wet-Chemical Synthesis of Doped Colloidal Nanoparticles: YVO_4:Ln (Ln = Eu, Sm, Dy). *J. Phys. Chem. B* **1998**, *102*, 10129–10135. [CrossRef]
39. Huang, S.; Wang, Z.; Zhu, Q.; Shi, X.; Wang, X.; Li, X.; Sun, X.; Li, J.G. A New Protocol for Templated Synthesis of YVO_4:Ln Luminescent Crystallites (Ln = Eu, Dy, Sm). *J. Alloys Compd.* **2019**, *776*, 773–781. [CrossRef]
40. Li, L.; Zhao, M.; Tong, W.; Guan, X.; Li, G.; Yang, L. Preparation of Cereal-like YVO_4:Ln^{3+} (Ln = Sm, Eu, Tb, Dy) for High Quantum Efficiency Photoluminescence. *Nanotechnology* **2010**, *21*, 195601. [CrossRef] [PubMed]
41. Mahata, M.K.; Koppe, T.; Hofsäss, H.; Kumar, K.; Vetter, U. *Host Sensitized Luminescence and Time-Resolved Spectroscopy of YVO_4: Ho^{3+} Nanocrystals*; Elsevier: Amsterdam, The Netherlands, 2015; Volume 76. [CrossRef]
42. Kalinichev, A.A.; Kurochkin, M.A.; Golyeva, E.V.; Kurochkin, A.V.; Lähderanta, E.; Mikhailov, M.D.; Kolesnikov, I.E. Near-Infrared Emitting YVO_4:Nd^{3+} Nanoparticles for High Sensitive Fluorescence Thermometry. *J. Lumin.* **2018**, *195*, 61–66. [CrossRef]
43. Pankratov, V.; Popov, A.I.; Shirmane, L.; Kotlov, A.; Feldmann, C. $LaPO_4$:Ce,Tb and YVO_4:Eu Nanophosphors: Luminescence Studies in the Vacuum Ultraviolet Spectral Range. *J. Appl. Phys.* **2011**, *110*, 5. [CrossRef]
44. Erdei, S.; Ainger, F.W.; Ravichandran, D.; White, W.B.; Cross, L.E. Preparation of Eu^{3+}: YVO_4 Red and Ce^{3+}, Tb^{3+}: $LaPO_4$ Green Phosphors by Hydrolyzed Colloid Reaction (HCR) Technique. *Mater. Lett.* **1997**, *30*, 389–393. [CrossRef]
45. Perala, R.S.; Singh, B.P.; Putta, V.N.K.; Acharya, R.; Ningthoujam, R.S. Enrichment of Crystal Field Modification via Incorporation of Alkali K^+ Ions in YVO_4:Ho^{3+}/Yb^{3+} nanophosphor and Its Hybrid with Superparamagnetic Iron Oxide Nanoparticles for Optical, Advanced Anticounterfeiting, Uranyl Detection, and Hyperthermia Applicati. *ACS Omega* **2021**, *6*, 19517–19528. [CrossRef] [PubMed]
46. Perala, R.S.; Joshi, R.; Singh, B.P.; Putta, V.N.K.; Acharya, R.; Ningthoujam, R.S. Brilliant Nonlinear Optical Response of Ho^{3+} and Yb^{3+} activated YVO_4 nanophosphor and Its Conjugation with Fe_3O_4 for Smart Anticounterfeit and Hyperthermia Applications. *ACS Omega* **2021**, *6*, 19471–19483. [CrossRef]
47. Runowski, M.; Wozny, P.; Stopikowska, N.; Martín, I.R.; Lavín, V.; Lis, S. Luminescent Nanothermometer Operating at Very High Temperature-Sensing up to 1000 K with Upconverting Nanoparticles (Yb^{3+}/Tm^{3+}). *ACS Appl. Mater. Interfaces* **2020**, *12*, 43933–43941. [CrossRef]

48. Buissette, V.; Huignard, A.; Gacoin, T.; Boilot, J.P.; Aschehoug, P.; Viana, B. Luminescence Properties of YVO_4:Ln (Ln = Nd, Yb, and Yb-Er) Nanoparticles. *Surf. Sci.* **2003**, *532–535*, 444–449. [CrossRef]
49. Sun, J.; Zhu, J.; Liu, X.; Du, H. Bright White Up-Conversion Emission from Er^{3+}/Ho 3+/Tm^{3+}/Yb^{3+} Co-Doped YVO_4 Phosphors. *Mater. Res. Bull.* **2013**, *48*, 2175–2179. [CrossRef]
50. Sobczyk, M. Influence of Nd^{3+} Concentration on Up-Conversion Fluorescence Colour in YVO_4 Co-Doped with Ho^{3+}, Yb^{3+} and Nd^{3+} Ions. *Mater. Lett.* **2012**, *88*, 86–88. [CrossRef]
51. Meng, Q.; Liu, T.; Dai, J.; Sun, W. Study on Optical Temperature Sensing Properties of YVO_4:Er^{3+}, Yb^{3+} Nanocrystals. *J. Lumin.* **2016**, *179*, 633–638. [CrossRef]
52. Zharkov, D.K.; Shmelev, A.G.; Leontyev, A.V.; Nikiforov, V.G.; Lyadov, N.M.; Lobkov, V.S.; Samartsev, V.V.; Saiko, A.P.; Hemmer, P.R. Luminescence Properties of YVO_4:Yb, Er Nanoparticles Dispersed in Water. *J. Phys. Conf. Ser.* **2019**, *1283*, 012015. [CrossRef]
53. Shyichuk, A.; Câmara, S.S.; Weber, I.T.; Carneiro Neto, A.N.; Nunes, L.A.O.; Lis, S.; Longo, R.L.; Malta, O.L. Energy Transfer Upconversion Dynamics in YVO_4:Yb^{3+}, Er^{3+}. *J. Lumin.* **2016**, *170*, 560–570. [CrossRef]
54. Kshetri, Y.K.; Regmi, C.; Kim, H.S.; Lee, S.W.; Kim, T.H. Microwave Hydrothermal Synthesis and Upconversion Properties of Yb^{3+}/Er^{3+} Doped YVO_4 Nanoparticles. *Nanotechnology* **2018**, *29*, 204004. [CrossRef]
55. Liang, Y.; Sun, K.; Wang, W.; Chui, P.; Sun, X. Hydrothermal Synthesis and Characterization of YVO_4:Yb^{3+}, Er^{3+} Microspheres. *Mater. Lett.* **2012**, *79*, 125–127. [CrossRef]
56. Yang, K.; Zheng, F.; Wu, R.; Li, H.; Zhang, X. Upconversion Luminescent Properties of YVO_4:Yb^{3+}, Er^{3+} Nano-Powder by Sol-Gel Method. *J. Rare Earths* **2006**, *24*, 162–166. [CrossRef]
57. Woźny, P.; Runowski, M.; Lis, S. Emission Color Tuning and Phase Transition Determination Based on High-Pressure up-Conversion Luminescence in YVO_4:Yb^{3+}, Er^{3+} Nanoparticles. *J. Lumin.* **2019**, *209*, 321–327. [CrossRef]
58. Szczeszak, A.; Runowski, M.; Wiglusz, R.J.; Grzyb, T.; Lis, S. Up-Conversion Green Emission of Yb^{3+}/Er^{3+} Ions Doped YVO_4 Nanocrystals Obtained via Modified Pechini's Method. *Opt. Mater.* **2017**, *74*, 128–134. [CrossRef]
59. Partl, G.J.; Hackl, I.; Götsch, T.; Penner, S.; Tribus, M.; Weinberger, N.; Petschnig, L.L.; Schildhammer, D.; Fuhrmann, G.L.; Huppertz, H.; et al. High Temperature Stable Bismuth Vanadate Composite Pigments via Vanadyl-Exchanged Zeolite Precursors. *Dye. Pigment.* **2017**, *147*, 106–112. [CrossRef]
60. Kimani, M.M.; Chen, H.; McMillen, C.D.; Anker, J.N.; Kolis, J.W. Synthetic and Spectroscopic Studies of Vanadate Glaserites I: Upconversion Studies of Doubly Co-Doped (Er, Tm, or Ho):Yb:$K_3Y(VO_4)_2$. *J. Solid State Chem.* **2015**, *226*, 312–319. [CrossRef]
61. Range, K.J.; Zintl, R.; Heyns, A.M. The Thermal Decomposition of Ammonium Metavanadate(V) in Open and Closed Systems. *Z. Nat. B* **1988**, *43*, 309–317. [CrossRef]
62. Kaczorowska, N.; Szczeszak, A.; Lis, S. Synthesis and Tunable Emission Studies of New Up-Converting $Ba_2GdV_3O_{11}$ Nanopowders Doped with Yb^{3+}/Ln^{3+} (Ln^{3+} = Er^{3+}, Ho^{3+}, Tm^{3+}). *J. Lumin.* **2018**, *200*, 59–65. [CrossRef]
63. Stopikowska, N.; Runowski, M.; Skwierczyńska, M.; Lis, S. Improving Performance of Luminescent Nanothermometers Based on Non-Thermally and Thermally Coupled Levels of Lanthanides by Modulating Laser Power. *Nanoscale* **2021**, *13*, 14139–14146. [CrossRef]
64. Tong, Y.; Zhang, W.; Wei, R.; Chen, L.; Guo, H. $Na_2YMg_2(VO_4)_3$:Er^{3+},Yb^{3+} phosphors: Up-conversion and optical thermometry. *Ceram. Int.* **2021**, *47*, 2600–2606. [CrossRef]
65. Sheldon, R.A. Fundamentals of Green Chemistry: Efficiency in Reaction Design. *Chem. Soc. Rev.* **2012**, *41*, 1437–1451. [CrossRef] [PubMed]
66. Anastas, P.; Eghbali, N. Green Chemistry: Principles and Practice. *Chem. Soc. Rev.* **2010**, *39*, 301–312. [CrossRef]
67. Du, P.; Ran, W.; Hou, Y.; Luo, L.; Li, W. Eu^{3+}-Activated $NaGdF_4$ Nanorods for near-Ultraviolet Light-Triggered Indoor Illumination. *ACS Appl. Nano Mater.* **2019**, *2*, 4275–4285. [CrossRef]
68. Du, P.; Ran, W.; Li, W.; Luo, L.; Huang, X. Morphology Evolution of Eu^{3+}-Activated $NaTbF_4$ Nanorods: A Highly-Efficient near-Ultraviolet Light-Triggered Red-Emitting Platform towards Application in White Light-Emitting Diodes. *J. Mater. Chem. C* **2019**, *7*, 10802–10809. [CrossRef]
69. Li, Y.C.; Chang, Y.H.; Lin, Y.F.; Lin, Y.J.; Chang, Y.S. High Color Purity Phosphors of $LaAlGe_2O_7$ Doped with Tm^{3+} and Er^{3+}. *Appl. Phys. Lett.* **2006**, *89*, 5–8. [CrossRef]
70. Wang, X.; Zhao, Z.; Wu, Q.; Wang, C.; Wang, Q.; Yanyan, L.; Wang, Y. Structure, Photoluminescence and Abnormal Thermal Quenching Behavior of Eu^{2+}-Doped $Na_3Sc_2(PO_4)_3$: A Novel Blue-Emitting Phosphor for n-UV LEDs. *J. Mater. Chem. C* **2016**, *4*, 8795–8801. [CrossRef]
71. Liang, Y.; Chui, P.; Sun, X.; Zhao, Y.; Cheng, F.; Sun, K. Hydrothermal Synthesis and Upconversion Luminescent Properties of YVO_4:Yb^{3+},Er^{3+} Nanoparticles. *J. Alloys Compd.* **2013**, *552*, 289–293. [CrossRef]
72. Liu, Y.; Yang, Q.; Ren, G.; Xu, C.; Zhang, Y. Relationship between microstructure and the achieving of the single-band red upconversion fluorescence of Er^{3+}/Yb^{3+} codoped crystallites. *J. Alloys Compd.* **2009**, *467*, 351–356. [CrossRef]
73. Yang, S.; Jiang, L.; Feng, J.; Li, J.; Chen, X.; He, M.; Chen, H. An Auto-Combustion Synthesis and Luminescence Properties of Polyhedral YVO_4: Ln^{3+} (Ln = Eu, Sm, Yb/Er, Yb/Tm) Microcrystals. *J. Mater. Res.* **2019**, *34*, 3636–3644. [CrossRef]
74. Su, X.Q.; Yan, B. In Situ Chemical Co-Precipitation Synthesis of YVO_4:RE (RE = Dy^{3+}, Sm^{3+}, Er^{3+}) Phosphors by Assembling Hybrid Precursors. *J. Non. Cryst. Solids* **2005**, *351*, 3542–3546. [CrossRef]
75. Huang, P.; Chen, D.; Wang, Y. Host-Sensitized Multicolor Tunable Luminescence of Lanthanide Ion Doped One-Dimensional YVO_4 Nano-Crystals. *J. Alloys Compd.* **2011**, *509*, 3375–3381. [CrossRef]

76. Medvedev, V.A.; Mamonova, D.V.; Kolesnikov, I.E.; Khokhlova, A.R.; Mikhailov, M.D.; Manshina, A.A. Synthesis and Luminescence Properties of YVO_4: Nd^{3+}, Er^{3+} and Tm^{3+} Nanoparticles. *Inorg. Chem. Commun.* **2020**, *118*, 107990. [CrossRef]
77. Xu, Z.; Kang, X.; Li, C.; Hou, Z.; Zhang, C.; Yang, D.; Li, G.; Lin, J. Ln^{3+} (Ln = Eu, Dy, Sm, and Er) Ion-Doped YVO_4 Nano/Microcrystals with Multiform Morphologies: Hydrothermal Synthesis, Growing Mechanism, and Luminescent Properties. *Inorg. Chem.* **2010**, *49*, 6706–6715. [CrossRef] [PubMed]
78. Yu, H.; Tian, Z.; Wang, H.; Chen, B.; Sun, J.; Cheng, L.; Li, X.; Zhang, J.; Xu, S. Electrospinning-Derived YVO_4:Er/Yb Nanowires and Nanotubes with Temperature Sensitivity of Their up-Converted Emission. *Ceram. Int.* **2021**, *47*, 25777–25784. [CrossRef]
79. Mialon, G.; Türkcan, S.; Dantelle, G.; Collins, D.P.; Hadjipanayi, M.; Taylor, R.A.; Gacoin, T.; Alexandrou, A.; Boilot, J.P. High Up-Conversion Efficiency of YVO_4:Yb,Er Nanoparticles in Water down to the Single-Particle Level. *J. Phys. Chem. C* **2010**, *114*, 22449–22454. [CrossRef]
80. Alkahtani, M.; Alfahd, A.; Alsofyani, N.; Almuqhim, A.A.; Qassem, H.; Alshehri, A.A.; Almughem, F.A.; Hemmer, P. Photostable and Small YVO_4:Yb,Er Upconversion Nanoparticles in Water. *Nanomaterials* **2021**, *11*, 1535. [CrossRef] [PubMed]
81. Zharkov, D.K.; Shmelev, A.G.; Latypov, I.Z.; Leontyev, A.V.; Nikiforov, V.G.; Lobkov, V.S.; Fedotov, I.V.; Alkahtani, M.H.; Hemmer, P.R.; Samartsev, V.V.; et al. Monitoring of the Luminescence Properties of the Upconversion YVO_4:Yb, Er Nanoparticles during Preparation Processes. *J. Phys. Conf. Ser.* **2020**, *1628*, 012012. [CrossRef]
82. Letters, L.P. Light Converting Yb^{3+} / Er^{3+} Doped YVO_4 Nanoparticles for Biological Applications. *Laser Phys.* **2020**, *17*, 075901. [CrossRef]
83. Yin, W.; Zhou, L.; Gu, Z.; Tian, G.; Jin, S.; Yan, L.; Liu, X.; Xing, G.; Ren, W.; Liu, F.; et al. Lanthanide-Doped $GdVO_4$ Upconversion Nanophosphors with Tunable Emissions and Their Applications for Biomedical Imaging. *J. Mater. Chem.* **2012**, *22*, 6974–6981. [CrossRef]
84. Kuznetsov, S.; Ermakova, Y.; Voronov, V.; Fedorov, P.; Busko, D.; Howard, I.A.; Richards, B.S.; Turshatov, A. Up-Conversion Quantum Yields of SrF_2:Yb^{3+},Er^{3+} Sub-Micron Particles Prepared by Precipitation from Aqueous Solution. *J. Mater. Chem. C* **2018**, *6*, 598–604. [CrossRef]
85. Saleta Reig, D.; Grauel, B.; Konyushkin, V.A.; Nakladov, A.N.; Fedorov, P.P.; Busko, D.; Howard, I.A.; Richards, B.S.; Resch-Genger, U.; Kuznetsov, S.V.; et al. Upconversion Properties of SrF_2:Yb^{3+},Er^{3+} Single Crystals. *J. Mater. Chem. C* **2020**, *8*, 4093–4101. [CrossRef]
86. Lu, D.; Mao, C.; Cho, S.K.; Ahn, S.; Park, W. Experimental Demonstration of Plasmon Enhanced Energy Transfer Rate in $NaYF_4$:Yb^{3+},Er^{3+} Upconversion Nanoparticles. *Sci. Rep.* **2016**, *6*, 1–11. [CrossRef] [PubMed]
87. Lim, C.S.; Aleksandrovsky, A.S.; Molokeev, M.S.; Oreshonkov, A.S.; Ikonnikov, D.A.; Atuchin, V.V. Triple Molybdate Scheelite-Type Upconversion Phosphor $NaCaLa(MoO_4)_3$:Er^{3+}/Yb^{3+}: Structural and Spectroscopic Properties. *Dalt. Trans.* **2016**, *45*, 15541–15551. [CrossRef] [PubMed]
88. Lim, C.S.; Atuchin, V.; Aleksandrovsky, A.; Molokeev, M.; Oreshonkov, A. Microwave Sol-Gel Synthesis of $CaGd_2(MoO_4)_4$:Er^{3+}/Yb^{3+} Phosphors and Their Upconversion Photoluminescence Properties. *J. Am. Ceram. Soc.* **2015**, *98*, 3223–3230. [CrossRef]
89. Pollnau, M.; Gamelin, D.; Lüthi, S.; Güdel, H.; Hehlen, M. Power Dependence of Upconversion Luminescence in Lanthanide and Transition-Metal-Ion Systems. *Phys. Rev. B—Condens. Matter Mater. Phys.* **2000**, *61*, 3337–3346. [CrossRef]
90. Lei, Y.; Song, H.; Yang, L.; Yu, L.; Liu, Z.; Pan, G.; Bai, X.; Fan, L. Upconversion Luminescence, Intensity Saturation Effect, and Thermal Effect in Gd_2O_3: Er^{3+}, Yb^{3+} Nanowires. *J. Chem. Phys.* **2005**, *123*, 174710. [CrossRef] [PubMed]
91. León-Luis, S.F.; Rodríguez-Mendoza, U.R.; Lalla, E.; Lavín, V. Temperature Sensor Based on the Er^{3+} Green Upconverted Emission in a Fluorotellurite Glass. *Sens. Actuators B Chem.* **2011**, *158*, 208–213. [CrossRef]